Links between the mountain torque and the Arctic Oscillation in the Laboratoire de Météorologie Dynamique (LMDz), general circulation model

F. Lott, L. Goudard, and A. Martin

Laboratoire de Météorologie Dynamique, CNRS/IPSL, Ecole Normale Supérieure, Paris, France

Received 13 April 2005; revised 7 July 2005; accepted 1 September 2005; published 29 November 2005.

[1] Recent papers suggest that in the National Center for Environmental Prediction (NCEP) reanalysis data there is a dynamical link between the mountain torque and the Arctic Oscillation (AO) at periodicities near and below 30 days. This link essentially occurs because the AO is associated with a redistribution of mass from the polar regions to the midlatitudes, hence giving a substantial contribution to the mass term of the atmospheric angular momentum (AAM). These results are confirmed here by using a 30-year simulation done with the Laboratoire de Météorologie Dynamique, zoom (LMDz), general circulation model. In particular, we verify that the changes in mass AAM occurring during intraseasonal variations of the AO are in good part driven by the mountain torque in the model also. In this respect, the LMDz model has the great advantage of closing the AAM budget nearly exactly, which is not the case with the NCEP reanalysis data. As the Antarctic Oscillation (AAO) is also associated with a redistribution of mass from the polar regions to the midlatitudes, its contribution to the AAM budget is also presented. As there are many fewer mountains in the Southern Hemisphere, we show that in the model as well as in the reanalysis the changes in mass AAM during intraseasonal variations of the AAO are in good part equilibrated by changes of opposite sign in wind AAM. The main interest of these results is that the mountain torque drives the changes in AAM, so it can sometimes participate actively in changes of the AO. It has a predictive value that is significant but small, around 10–15% for periodicities near and below one month, while a good fraction of the AO variability occurs at longer timescales.

Citation: Lott, F., L. Goudard, and A. Martin (2005), Links between the mountain torque and the Arctic Oscillation in the Laboratoire de Météorologie Dynamique (LMDz), general circulation model, *J. Geophys. Res.*, *110*, D22107, doi:10.1029/2005JD006073.

1. Introduction and Motivation

[2] During the last three decades, considerable research has been carried out on the low-frequency variability of the atmosphere. In the extratropics, *Blackmon* [1976], *Sawyer* [1976], and others have found that the variance of the 500-hPa geopotential height is larger for the low-frequency part of the spectrum, with periods longer than 10 days, than for the higher-frequency part. This low-frequency variability is essentially contained in the planetary scales and is dominated by a few spatial patterns that can be effectively extracted by principal components analysis [*Preisendorfer*, 1988; *Molteni et al.*, 1990]. The leading patterns among these are the Arctic Oscillation (AO) in the Northern Hemisphere [*Wallace*, 2000] and the Antarctic Oscillation (AAO) in the Southern Hemisphere.

[3] Several theoretical explanations of extratropical low-frequency variability have been given. One of them follows the seminal work of *Charney and DeVore* [1979], who pointed out that in a low-order nonlinear quasi-geostrophic model, the interaction of the flow with large-scale topography can give rise to multiple equilibriums through topographic instability. More highly resolved models [*Legras and Ghil*, 1985; *Yoden*, 1985] produce more complex aspects of low-frequency variability, such as periodic and aperiodic solutions, suggesting that an oscillatory form of topographic instability also exists. Other mechanisms for the extratropical low-frequency variability have been proposed. Among them, the most efficient is the large-scale response to synoptic transient eddy forcing [*Hoskins et al.*, 1983; *Illari and Marshall*, 1983; *Vautard et al.*, 1988].

[4] The different theories of extratropical low-frequency variability are not mutually exclusive, and at least one aspect of the theory of oscillatory topographic instability is supported by observational evidence, namely, mountain torques due to traveling Rossby waves affect the zonal flow in the midlatitudes and substantially affect the AO. For instance, *Metz* [1985] has found significant cross-spectral peaks between the mountain torque T_M and the zonal wind at periodicities above 15 days. *Lejenäs and Madden* [2000] have found links between Rossby waves, mountain torque,

0148-0227/05/2005JD006073$09.00

and atmospheric angular momentum (AAM) in the 6–15-day band. More recently, *Lott et al.* [2004] have found that changes in the AO in the 20–30-day band are preceded by a small but significant signal in the mountain torque.

[5] The relationship between the mountain torque and the AO given by *Lott et al.* [2004] was established in three steps and using 40 years (1958–1998) of the National Center for Environmental Prediction (NCEP) reanalysis. In the first step, they extract the AO via a principal component analysis of low-troposphere variability in the Northern Hemisphere (NH) and evaluate the contribution of the mountains located in the NH to T_M. Then a cospectral analysis shows that the NH T_M and the AO are correlated at periodicities near and below 30 days, with the NH T_M in lead-lag quadrature with the AO. As the AO pattern is predominantly cyclonic in the polar region and anticyclonic in the midlatitudes and subtropics this picture is consistent with a positive T_M accelerating the midlatitude jet.

[6] In a second step, *Lott et al.* [2004] made composite maps of the circulation in the low troposphere according to the extrema in the NH T_M and in the AO index, both series being filtered to focus on the 20–30-day band. The composites are the average of maps corresponding to dates when the resulting series exceeds a given threshold, minus the average of maps corresponding to dates when the series is below minus the same threshold. At zero-day lag, the composite keyed to the NH T_M is cyclonic to the west of the Rockies and to the west of the Himalayas, and it is anticyclonic to the east of the Rockies and over the Himalayas. A positive T_M results from the east-west surface pressure gradients across the mountains associated with these patterns. Around a week before, the composite is a circulation pattern that is predominantly anticyclonic in the polar regions and northern midlatitudes and that is fairly zonally symmetric (hence projecting somehow on minus the AO). Around a week after, the composite is a circulation pattern that is predominantly cyclonic in the polar regions and northern midlatitudes (hence projecting on the AO). Conversely, composites keyed to the AO show that around a week after the AO, the large-scale circulation presents zonal pressure gradients over the Rockies and Himalayas that can produce a substantial NH T_M.

[7] In the last step, *Lott et al.* [2004] provide more quantitative evidence and analyze whether the NH T_M is substantial enough to move the AO back and forth. To do this, they evaluate the dynamical inertia of this pattern, for instance, the characteristic amplitude of the mass AAM (M_Ω) variations with which it is associated. They note that it is comparable with the characteristic amplitude of the variations of M_Ω seen in the reanalysis. More precisely, an examination of the AAM budget during the variations of the AO in the 20–30-day band shows that when the AO varies, M_Ω varies and is nearly entirely driven by the NH T_M.

[8] The *Lott and D'Andrea* [2005] paper is more dynamical and tries to explain why the mass AAM is so central during the AO compared to the wind AAM (M_R). In it, it is shown that at periodicities below 25 days the AAM response to mountain torques is equally made of mass angular momentum and wind angular momentum (M_R), the partition between the two being controlled by the geostrophic balance: When T_M is produced by mountains located in the polar regions, M_Ω is larger than M_R in the response; when T_M is produced by mountains located in the tropics, M_Ω is smaller than M_R; and $M_R \approx M_\Omega$ when T_M is produced by mountains located in the midlatitudes. These results are supported by a simple model for geostrophic adjustment on the sphere. According to these findings, and considering that the AO is a circulation pattern confined to the polar regions, it is natural that its relationships with T_M occur via M_Ω rather than via M_R. Note also that this is consistent with *von Storch* [1994, 1999], who found in a coupled general circulation model (GCM) that two among the three dominant modes of large-scale variability are associated with larger M_Ω than M_R variations.

[9] The results given by *Lott et al.* [2004] and *Lott and D'Andrea* [2005] have two weak points. The first is that the reanalysis data are not entirely dynamically consistent: They mix analyzed products of wind and surface pressure to evaluate M_R, M_Ω, and T_M with short-range forecasts of the surface friction to evaluate the frictional torque T_B. Even if the NCEP model were closing the AAM budget perfectly, the mixture of observations and forecasts made to produce the requested fields induces imbalances in the AAM budget. In this respect, the results of *Huang et al.* [1999] are particularly instructive. They noted that the inclusion of the gravity wave drag in the evaluation of the total torque degrades the AAM budget closure in the NCEP data. The second weak point of the results given by *Lott et al.* [2004] and *Lott and D'Andrea* [2005] is that the coherencies found between the mountain torque and the AO are in general below 0.4, even for the periodicities below 30 days, for which the coherency is the best. Although significant, these values are rather small and need to be cross-checked in a more dynamically consistent framework.

[10] Furthermore, the dynamical interpretation that T_M and the AO are linked via M_Ω given by *Lott et al.* [2004] and *Lott and D'Andrea* [2005] also needs to be tested by analyzing the AAM budget closure during variations of the Antarctic Oscillation. Indeed, the AAO also corresponds to a redistribution of mass from the polar latitudes to the midlatitudes and is consequently related to M_Ω variations. In this case, since there are many fewer mountains in the Southern Hemisphere, the changes in M_Ω during the AAO must be equilibrated by other processes, like opposite changes in wind angular momentum, or by the frictional torques. Again, to examine this, a dynamically consistent framework is extremely helpful.

[11] The plan of the paper is as follows. Section 2 contains a description of the model, its midlatitude sea level pressure (SLP) variability (which includes the analysis of the model's AO and AAO), and its AAM budget. Section 3 describes the links between T_M, the AO, and the AAO. In section 3.1 these links are evaluated using conventional spectral analysis techniques. In section 3.2 the links between T_M and the AO are interpreted comparing composites of SLP fields keyed to intraseasonal changes in T_M and in the AO. In section 3.3, composites of the AAM budget during intraseasonal changes of the AO and of the AAO are presented.

[12] In all sections the results from the model are compared with similar results from 30 years (1971–2000) of the National Center for Atmospheric Research (NCAR)/NCEP reanalysis [*Kalnay et al.*, 1996]. In some cases, the results from the reanalysis are very close to those described by *Lott*

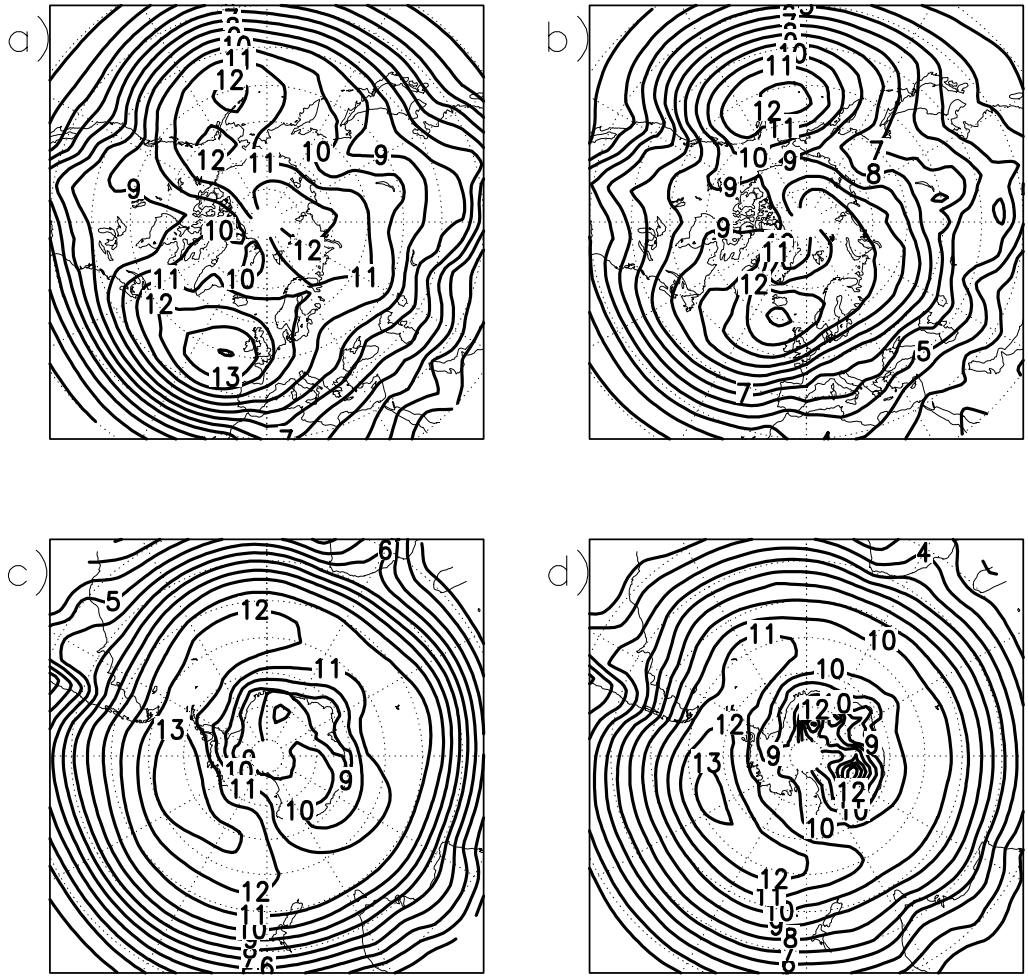

Figure 1. Standard deviation of sea level pressure daily variability, based on 30 years of data and after subtracting the annual cycle. (a) LMD GCM for the NH, (b) NCEP reanalysis for the NH, (c) LMD GCM for the SH, and (d) NCEP reanalysis for the SH. Contour interval is 1 hPa.

et al. [2004] and *Lott and D'Andrea* [2005], so they will be described here very briefly.

2. Model Description

2.1. Variability in the Model Low Troposphere

[13] Our model data are derived from a 30-year simulation done with the Laboratoire de Météorologie Dynamique, zoom (LMDz), GCM developed at the Institute Paul and Simon Laplace. In this simulation the horizontal resolution is 2.5° × 2.5°, and there are 19 levels in the vertical direction, most of them in the troposphere (there are only 4 levels above 20 km). At the lower boundary the model is forced by sea surface temperatures and sea ice cover that vary during a climatological annual cycle. The model and its winter mean climatologies are described by *Lott* [1999]. Briefly, it has a realistic zonal mean flow and realistic steady planetary waves in the midlatitudes.

[14] Since we focus here on links between the mountain torque and the AO, it is important that the model produce a reasonable simulation of the troposphere variability. Figure 1a shows the root mean square of daily SLP variability from the model in the NH and after subtraction of the annual cycle. It reveals two major centers of action over the northeastern Pacific and the northeastern Atlantic that compare in amplitude with those from the reanalysis in Figure 1b. In the model these two centers of action are substantially broader than those in the reanalysis, in the sense that they extend farther over the midlatitudes. In particular, the model northeastern Atlantic center of action is almost 10° to the south of the corresponding center in the reanalysis. In the model a third center of action is present near the polar region north of Siberia. It is slightly more pronounced than the corresponding one in the reanalysis (Figure 1b).

[15] For the Southern Hemisphere (SH) (Figure 1c) the SLP has enhanced variance over a broad sector between the latitudes 40°S and 20°S and that covers half the hemisphere in longitude almost entirely to the west of the Greenwich meridian. This pattern of enhanced variance is again realistic in shape, zonal extension, and location when compared to the reanalysis in Figure 1d. As for the NH, it extends slightly too much toward the equator.

[16] The dominant patterns of atmospheric variability in the midlatitudes are captured here by projecting the sea level pressure onto the leading spatial empirical orthogonal functions (EOFs) [*Preisendorfer*, 1988]. We compute EOFs over NH and SH separately, i.e., north of 30°N and south of

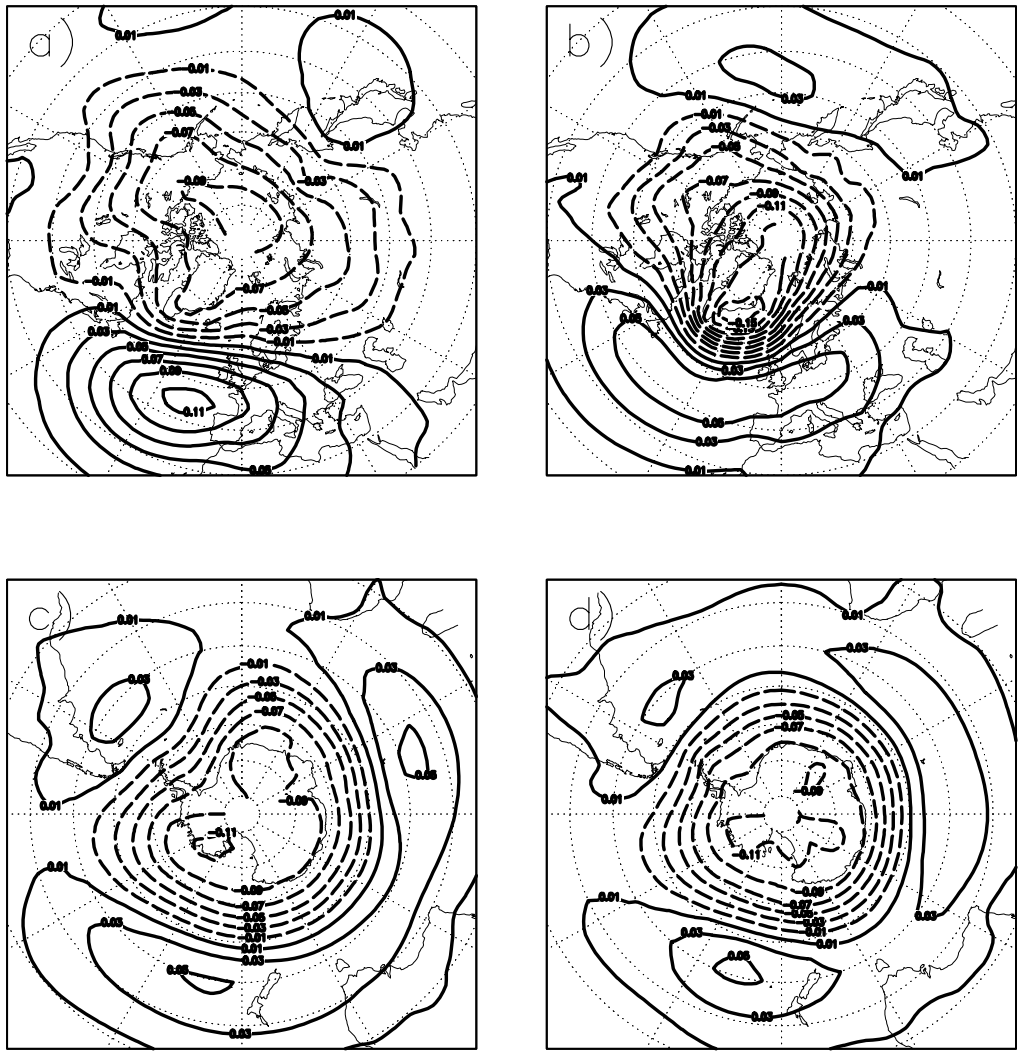

Figure 2. Leading EOF of hemispheric daily variability, based on 30 years of data and after subtracting the annual cycle. (a) LMD GCM for the NH, (b) NCEP reanalysis for the NH, (c) LMD GCM for the SH, and (d) NCEP reanalysis for the SH. Contour interval is 0.02, and negative values are shown with dashed contours.

30°S, respectively, again after subtraction of the annual cycle. We repeat the same analysis for the NCEP data.

[17] The first model NH EOF (Figure 2a) accounts for 10.5% of the SLP daily variance. It is fairly zonally symmetric and exhibits a change in sign in the midlatitudes, with one extensive and intense negative feature spreading all over the Arctic and one strong positive center over the North Atlantic. It resembles the same leading EOF in the reanalysis (Figure 2b, 8.9% of the variance), but with three noticeable differences. The broad negative center of action covering the polar region in the EOF 1 from the reanalysis does not extend much to the south of the 50°N latitude, while in the model it goes well beyond that over central Eurasia and the northeastern Pacific. This difference is a consequence of the fact that the centers of action for SLP variability extend too much equatorward in the model (Figures 1a and 1b). Note also that the reanalysis EOF 1 presents a positive center over the central North Pacific Ocean that is practically absent in the model. Still, in the reanalysis, the minimum over the Greenland is more pronounced than in the model.

[18] For the SH the first model EOF (Figure 2c) accounts for 10.9% of the SLP daily variance and corresponds to a reinforcement of the midlatitude jet. In this respect, it compares well with the AAO in the reanalysis (Figure 2d, 10.4% of the variance). Nevertheless, it is less zonally symmetric than in the reanalysis and presents a ridge near the Greenwich meridian that is absent from the reanalysis.

[19] Despite their differences from the NCEP data the first two EOFs of the model essentially correspond to reinforced westerly jets all around the midlatitudes (as do the AO and the AAO). They also correspond to a redistribution of mass from the polar latitudes toward the midlatitudes and the subtropics, which can make them contribute to changes in M_Ω.

2.2. AAM Budget Closure

[20] The global AAM tendency budget is given by

$$\frac{dM}{dt} = \frac{d(M_R + M_\Omega)}{dt} = T_M + T_B + T_S = T, \qquad (1)$$

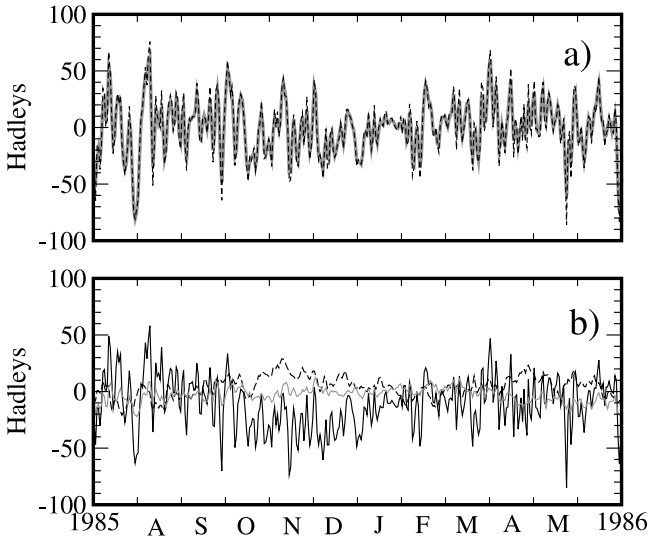

Figure 3. Model atmospheric angular momentum balance and torques over 1 year. (a) Global AAM tendency (thick grey line) and total torque (dashed line). (b) Mountain torque (black line), frictional torque (dashed line), and subgrid-scale orography torque (grey line).

where

$$M_R = \int_V \rho r \cos\theta u \, dV \ , \quad M_\Omega = \int_S \Omega r^2 \cos^2\theta \frac{P_s}{g} dS, \qquad (2)$$

and

$$T_M = -\int_S P_s \frac{\partial Z_s}{\partial \lambda} dS \ , \ T_B = \int_S r \cos\theta \tau_B \, dS \quad \text{and} \quad T_S = \int_S r \cos\theta \tau_S \, dS. \qquad (3)$$

Here M and T are the absolute atmospheric angular momentum and the total torque, while M_R, M_Ω, T_M, T_B, and T_S are the wind angular momentum, the mass angular momentum, the torque due to the mountains, the torque due to the surface friction τ_B, and the torque due to the subgrid-scale orographic drag τ_S (for the LMDz GCM, see *Lott and Miller* [1997] and *Lott* [1999]). In equations (2) and (3), $\int_V dV$ is the integral over the volume atmosphere, and $\int_S dS$ is the integral over the Earth surface. ρ is the density, λ is the longitude, θ is the latitude, r is the radius of the Earth, Ω is the angular velocity of Earth's rotation, Z_s is the topographic height, and P_s is the surface pressure. In the LMDz GCM, they are evaluated online every 15 min, at each physical parameterization step. After this online evaluation, daily averages of these five quantities are formed.

[21] Figure 3a shows the global AAM budget for the model year 1985 expressed in Hadleys (1 H = 10^{18} kg $m^2 s^{-2}$) and from the daily series. The tendency dM/dt matches almost perfectly the total torque, the correlation between T and dM/dt being around $r = 0.98$. This is the major advantage of using model data rather than reanalysis data: In the NCEP reanalysis the correlation between T and dM/dt is around $r = 0.87$ [*Lott et al.*, 2004].

[22] Figure 3b compares T_M, T_B, and T_S and shows that the mountain torque presents substantially larger fluctuations than T_B. They also occur on a faster timescale (as in the NCEP reanalysis; *Lott et al.* [2004]). Note as well that the torque due to the subgrid-scale orographic drag is rather small compared to both T_M and T_B. In the rest of this paper we will not discuss the role of T_S. The first justification for this is that it is a small term that can be integrated to T_M or T_B without affecting the results. A second justification is that we only discuss here the torque due to the large-scale mountains, to support the findings of *Lott et al.* [2004]. It is also justified by the fact that in the reanalysis data, T_S degrades the AAM budget balance and is always omitted [*Huang et al.*, 1999].

3. Links Between the Mountain Torque and the Leading Modes of Midlatitude Variability

3.1. Spectral Analysis

[23] To evaluate at which frequencies the mountain torque, the Arctic Oscillation, and the Antarctic Oscillation are related in the model, we perform here a conventional cross-spectral analysis between the corresponding series (Figure 4, see caption for details on the method). For the

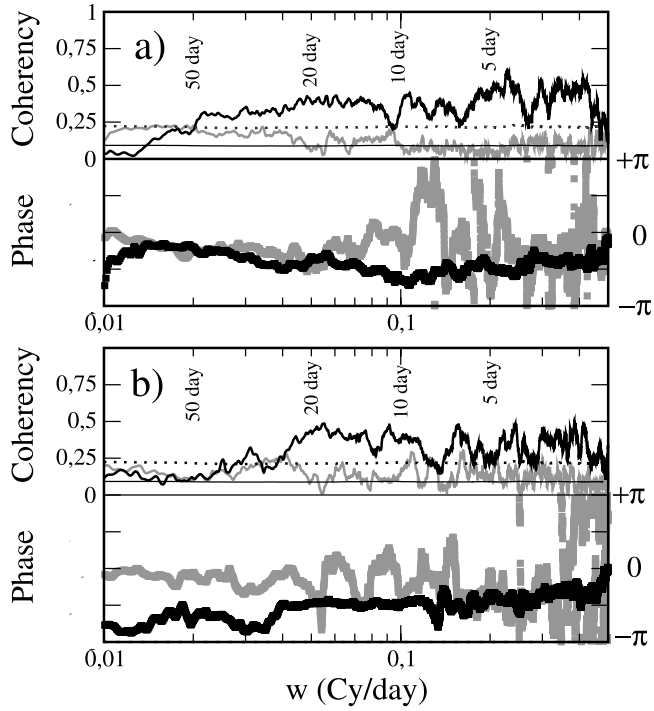

Figure 4. Cross-spectral analysis between the mountain torque and the AO (black lines) and the AAO (grey lines). (a) Results from the model and (b) results from the reanalysis. The upper panels in Figures 4a and 4b present the coherencies, and the lower panels are for the phases. In both Figures 4a and 4b the coherencies and phases are deduced from the cross periodograms and the periodograms of the series, each of them smoothed by a 100-point 10% cos window. In the frequency domain this yields a resolution of 10^{-2} cycles/d. For the coherencies the 1% confidence level is also displayed. It is evaluated via a Monte Carlo procedure, which uses an ensemble of 100 pairs of independent red noise series whose variance and lag 1 correlations correspond to those of T_M and of the PC 1.

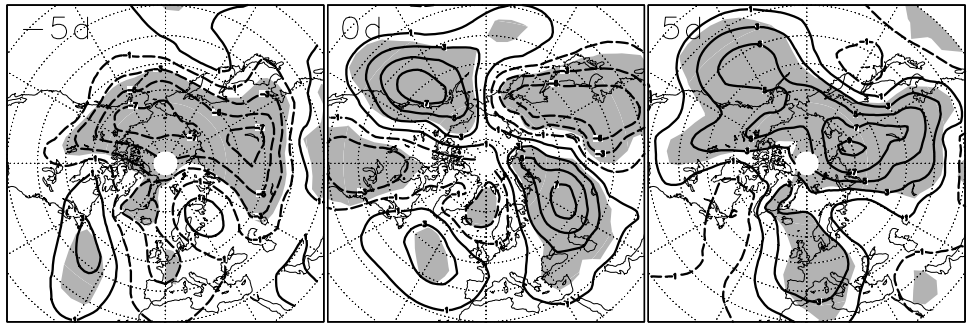

Figure 5. Composite of the IS sea level pressure fields keyed to minus the IS mountain torque. (a) −5-day lag, (b) 0-day lag, and (c) 5-day lag. Contour interval is 2 hPa: positive values, thick solid contours; negative values, thick dashed contours. The 1% confidence level is shaded. The days for each composite cycle are counted from the local extrema of the IS T_M.

AO index and for the AAO index we use the leading principal components (PC 1) issued from the EOF analysis in section 2.1. The black line in the top panel of Figure 4a presents the coherency between the mountain torque series and the AO index. It is above 0.25 and significant for nearly all periodicities below 50 days ($\omega > 0.02$ cycles/d). It is near 0.4 for periodicities below 20 days and approaches 0.5 at the end of the spectra (for $\omega > 0.2$ cycles/d). The phase (black line in the lower panel of Figure 4a) remains around $-\pi/2$, at least for all values of the frequency ω for which the coherency is significant. By contrast, the coherency between the mountain torque and the AAO index (grey line in the top panel of Figure 4a) is nearly never significant. It only approaches the 1% confidence levels for rather long periodicities, i.e., when $\omega < 0.02$ cycles/d.

[24] The same analysis for the NCEP data in Figure 4b shows that the spectral relationships between the mountain torque, the AO, and the AAO in the model are representative of those in the reanalysis. Note, however, that in the NCEP data the coherency between T_M and the AO index only becomes significant at periodicities below 33 days.

[25] The same cross-spectral analysis has been carried out between the mass angular momentum M_Ω, the AO, and the AAO (not shown). At nearly all frequencies in the model and in the reanalysis, M_Ω is in phase with the PC 1 series. In general, the coherencies are between 0.3 and 0.6 at all periodicities and always significant (for the NCEP data and the AO, see, for instance, Figure 2d of *Lott and D'Andrea* [2005]).

3.2. Composite Analysis of Sea Level Pressure Fields

[26] To explain the lead-lag relationships between the T_M and the AO in Figure 4, we can make four nonexclusive hypotheses. In two of them, T_M precedes the AO. In these cases, when T_M is positive (negative), it accelerates (decelerates) the zonal flow in the midlatitudes, a process that can lead to increase (decrease) of the AO signal at a later stage. In the other two hypotheses, T_M follows the AO: When the AO signal is positive (negative), it can return to a smaller (larger) values under the action of a positive (negative) T_M. To address which among these hypotheses is relevant for the surface climate, we have made a composite analysis of the sea level pressure maps keyed to the series of the mountain torque T_M and of the AO.

[27] To increase the statistical significance of our results, we next focus on the intraseasonal (IS) 10–150-day band. Although this band is rather large and often used in the literature [*Ghil and Mo*, 1991], this choice implies that we exclude from the composite analysis the interannual variability. This is justified by the fact that at long periodicities the friction torque dominates the mountain torque substantially [*Rosen*, 1993]. We also exclude the synoptic variability, which is dominated by the baroclinic eddies. This is justified by the fact that this variability is not well captured by the AO. Note also that the results given by *Lott et al.* [2004] concern the 20–30-day band and that the coherency in Figure 4a is only significant for periodicities below 50 days. These bounds guarantee that the IS band captures a large part of the relationships between the mountain torque and the AO we discuss here.

[28] To focus on the IS band, we follow *Ghil and Mo* [1991] and first apply to all series and maps the high-pass filter due to *Papoulis* [1973], which is defined by the minimum bias taper,

$$W_0(t) = \frac{1}{\pi}\left|\sin\frac{\pi t}{L}\right| + \left(1 - \frac{|t|}{L}\right)\cos\frac{\pi t}{L}, \text{ for } |t| < L; \qquad W_0(t) = 0, \text{for } |t| > L. \tag{4}$$

A choice of maximum lag $L = 90$ gives the half-power point of the frequency window associated with $W_0(t)$ at 150 days. To filter out the synoptic transient eddies, we next apply the low-pass filter developed by *Blackmon and Lau* [1980], whose half-power point is around 10 days. The resulting series are referred to as the IS series.

[29] Figures 5a–5c show the model composites of sea level pressure that are associated with negative values of the IS T_M. These composites are built from IS SLP maps selected when the IS T_M presents a local extremum whose amplitude is larger than a threshold value equal to 2.3 times the standard deviation of the IS T_M series ($\sigma(T_M)$). At zero lag, for instance (Figure 5b), the composite is the average of the IS SLP maps over the N^+ dates when the IS T_M has a local minimum that is smaller than $-2.3\ \sigma(T_M)$, minus the average of the IS SLP maps over the N^- dates when the IS T_M has a local maximum that is larger than $+2.3\ \sigma(T_M)$. The total number N of extrema in T_M selected in Figure 5 is $N = N^+ + N^- = 85$, with $N^+ = 50$ and $N^- = 35$. At a given

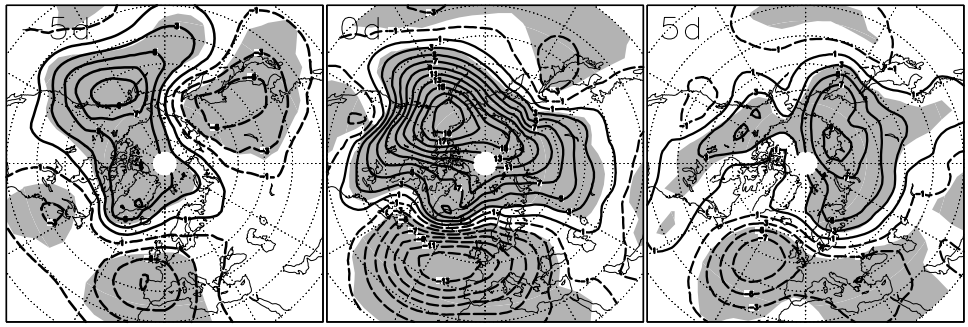

Figure 6. Same as Figure 5 but for composites keyed to minus the IS AO.

nonzero lag, composites are built with those maps that each correspond to a date situated at the given lag from the local extrema identified before in the IS T_M. The threshold value of 2.3 $\sigma(T_M)$ taken here is rather arbitrary; it ensures that between two and three dates are selected each year to build the composites. Note that we verified that the results are not very sensitive to moderate changes in this threshold. Areas that equal or exceed a 1% Student test for the significance are shaded.

[30] The choice to key our composites to minus the IS T_M rather than to the IS T_M is a complication that needs some comment. In the model it happens that there is a rather pronounced asymmetry between negative and positive extrema in the mountain torque, with substantially more minima then maxima (see Figure 3b). Predominantly, the model IS T_M becomes large and negative to decelerate the flow. We could have contrasted composite maps where the IS T_M is negative and maps where it is positive and discussed the difference. For brevity, and because we did not observe such a difference in the reanalysis data, we do not do this here. To summarize, the composite patterns in Figure 5 essentially result from negative values of the IS T_M, hence our choice here to key our composites to negative values in the corresponding series.

[31] At zero lag with respect to the extrema of T_M (Figure 5b), the composite essentially shows east-west dipoles over the Rockies and the Himalayas, respectively. Over both mountain massifs the composite pattern is positive to the west and negative to the east. According to this composite map a negative IS T_M is due to the zonal pressure differences over these two major massifs.

[32] The flow deceleration associated with negative IS T_M in the model is clearly substantial and significant before and after the extrema selected. At -5 day lag (Figure 5a) the flow in the NH is predominantly anticyclonic over nearly the whole polar region, while it is predominantly cyclonic at +5 day lag (Figure 5c). If we now compare the flow pattern in Figure 5a with the AO pattern in Figure 2a, there is a clear positive correlation. Conversely, the flow pattern in Figure 5c correlates with minus the AO pattern in Figure 2a. This result suggests that changes in the AO can be produced by the mountain torque, at least in part and from time to time.

[33] If this is true, the composites according to the IS AO must show patterns, at nonzero lag, that correlate well with the SLP pattern associated with a substantial torque in Figure 5b. This point is checked in Figure 6, which shows composites keyed to minus the IS AO. As for the composites keyed to the IS T_M, the maps selected correspond to days where the IS AO presents extrema that exceed 2.3 times the standard deviation of that series, yielding $N^+ = 40$ and $N^- = 42$. Before a negative extremum in the IS AO (Figure 6a), the sea level pressure clearly presents negative zonal gradients over the Rockies and the Himalayas that can lead to a negative torque. More precisely, over the Rockies, this negative gradient is due to the pattern of positive SLP centered over the northeastern Pacific, slightly to the south of the Alaskan peninsula in Figure 6a. The negative pressure gradient over the Himalayas is due to the pattern of negative SLP centered over eastern Asia in Figure 6a. The same patterns are clearly present in the composite that gives a large negative mountain torque in Figure 5b. Note also that after a negative extremum in the IS AO (Figure 6c) the SLP composite does not present clear zonal pressure gradients over the Rockies and the Himalayas: The mountain torque signal is presumably larger before the AO than after it.

[34] We have also made the composite maps in Figures 5 and 6 using the NCEP data (not shown). The results are very similar to those in Figure 5 and 9 of *Lott et al.* [2004], so we will not repeat their description here. The overall behavior of the model is comparable with that of the reanalysis. Nevertheless, in the reanalysis, the composites keyed to the IS T_M are equally due to the maxima and to the minima of the corresponding series. For those keyed to the IS AO the fact that they can give rise to a mountain torque at negative lag is even clearer in the reanalysis data than in the model. In the reanalysis also, the composite keyed to the IS AO at positive lag also presents patterns that can result in a mountain torque.

3.3. Composite Analysis of the AAM Budget

[35] To establish more quantitatively that the mountain torque can sometimes drive change in the AO, it is essential to notice that the AO pattern in Figure 2a corresponds to a redistribution of mass from the polar regions toward the midlatitudes and the tropics. It is thus associated with modifications in mass angular momentum, whose characteristic amplitude can be estimated by taking for the surface pressure in the estimation of M_Ω (equation (2)) the EOF pattern in Figure 2a. Then, multiplying the value obtained by the standard deviation of the PC 1, a characteristic value near 30 Hadley days (Hd) is obtained (1 Hd = $8.64\ 10^{22}$ kg $m^2\ s^{-1}$. As the standard deviation of M_Ω is around 70 Hd and as the changes in M_Ω are in good part driven by the mountain torque, it is clear that the mountain torque is large enough to move the AO back and forth.

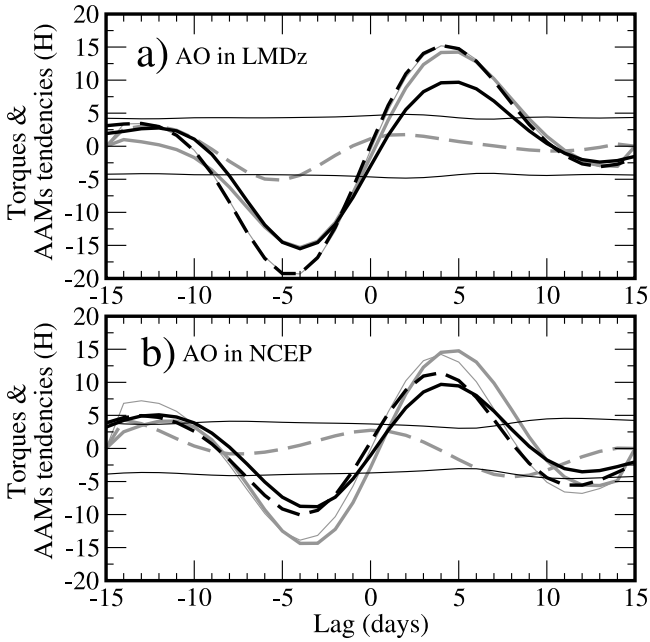

Figure 7. Composites of different terms in the AAM budget, keyed to minus the IS AO: (a) LMDz model and (b) NCEP reanalysis. IS M_Ω tendency (thick grey solid lines), IS M_R tendency (thick grey dashed lines), IS total AAM (M) tendency (thin grey lines), IS T_M (thick black solid lines), and IS total torque T (thick black dashed lines). The thin black lines are 1% confidence levels for the IS T_M, evaluated with a Student test with N degrees of freedom, N being the number of dates selected to build the composites.

[36] To support this more precisely, Figure 7a presents the evolution of the IS composites of different terms in the AAM budget keyed to minus the IS AO (the days selected are those used for the SLP composites in Figure 6). These composites are compared to composites of the AAM budget keyed to minus the IS AO in the NCEP data (Figure 7b, threshold equal to 2.3 times the standard deviation of the IS AO, yielding $N = 83$). In the composites from the model (Figure 7a) the mountain torque (T_M, thick black line) has a large and negative value below −15 H at −5 day lag. It becomes positive and near 10 H at +5 day lag. It follows well the composites of the total torque (T, thick black dashed line), witnessing the fact that the mountain torque is the major contributor to the AAM variations when the IS AO varies. It is important to note here that the mass AAM tendency (dM_Ω/dt, thick grey line) follows well the total AAM tendency (dM/dt, thin grey line). Both curves are very close to each other at positive lag and differ by less than 5 Hd at negative lag, a value that is marginally significant at the 1% confidence level. To summarize, when the AO varies in the model, the mass AAM varies as well, and the variations in mass AAM are essentially driven by the mountain torque.

[37] The fact that the model data support the results obtained from the reanalysis data is well illustrated comparing Figure 7a and Figure 7b. Overall, the model behaves in agreement with the observations, giving an independent and dynamically consistent confirmation that the mountain torque can affect the AO via the mass angular momentum. This confirmation was needed because in the NCEP data the composite of the AAM budget is not closed as well as the LMDz GCM is: The total torque and the AAM tendency match very well in Figure 7a; they do not in Figure 7b.

[38] As stated in section 1, another approach to evaluate the significance of the mountain torque for the AO dynamics is to compare AAM budget composites during variations of the IS AO and of the IS AAO. For the model IS AAO this is done in Figure 8a, where the composites are built selecting $N = 85$ dates when the IS AAO presents extrema that exceed 2.1 times its standard deviation. The thick grey line in Figure 8a shows that the mass AAM decreases before the IS AAO reaches a minimum ($dM_\Omega/dt < 0$ at negative lag) and increases after this minimum ($dM_\Omega/dt > 0$ at positive lag). These tendencies in M_Ω are associated with comparable tendencies in total angular momentum M, but the amplitudes of the extrema in dM/dt (thin grey line) are less pronounced than those in dM_Ω/dt. The extrema in dM/dt also present a delay of 2–3 days compared to those in dM_Ω/dt. These differences in amplitude and phase have two origins. First, a substantial fraction of the dM_Ω/dt variations are equilibrated by variations of opposite sign in dM_R/dt (thick grey dashed line in Figure 8a). Second, the torques (T_M and T, thick black solid line and thick black dashed line, respectively) peak at rather small negative lag. In this circumstance it is much more difficult than it is for the AO to say that the mountain torque T_M drives the changes in M_Ω because the M_Ω tendency and the mountain torque are closer to being in quadrature than in phase.

[39] It is again important to note that the behavior of the AAM budget during IS variations of the model AAO represents well that in the NCEP reanalysis (Figure 8b, same value for the threshold as in Figure 8a, yielding $N = 82$). Also, in the reanalysis, the changes in mass AAM occurring during variations of the AAO (dM_Ω/dt, thick grey line) are in good part equilibrated by changes of opposite

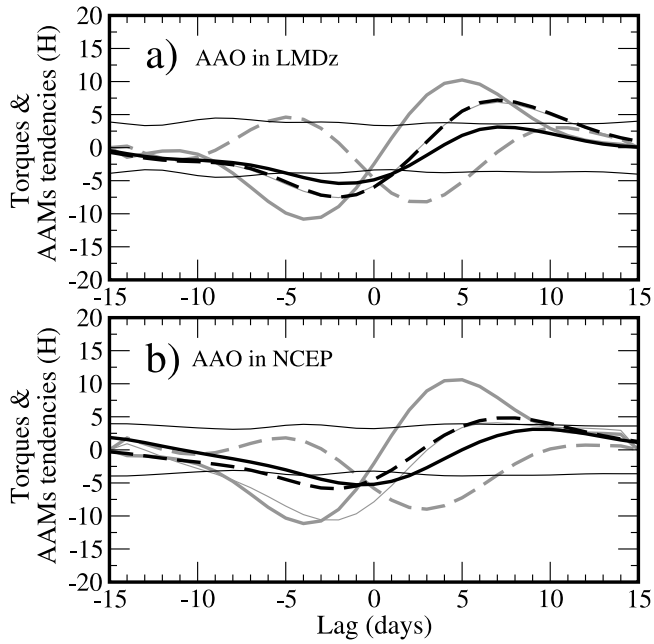

Figure 8. Same as Figure 7 but for the Antarctic Oscillation.

sign in wind AAM (dM_R/dt, thick grey dashed line), with the torques being more passive than for the AO. Nevertheless, in the composites from the reanalysis (Figure 8b), there are large errors between dM/dt (thin grey line) and T (thick black dashed). Hence the fact that the changes in mass AAM are in good part equilibrated by changes of opposite sign in M_R is much more difficult to assess. The fact that this balance occurs without ambiguity in the model helps us to conclude that this equilibration is likely to occur in reality as well.

4. Conclusion

[40] A 30-year integration done with the tropospheric version of the atmospheric GCM LMDz has been used to analyze the links between the mountain torque and the Arctic Oscillation. The model results have been systematically compared with those from the NCEP reanalysis, which have been extensively discussed elsewhere [*Lott et al.*, 2001, 2004; *Lott and D'Andrea*, 2005]. To control that, the LMDz model is adapted for this purpose; we have first verified that it has a reasonable intraseasonal variability in sea level pressure fields (Figure 1). In particular, its leading modes of variability in the NH and in the SH are reminiscent of the Arctic Oscillation and of the Antarctic Oscillation, respectively (Figure 2). Second, we have verified that the model closes the AAM budget perfectly (Figure 3a).

[41] To detect possible links between the mountain forcing and the AO, we have first proceeded to a cross-spectral analysis between the mountain torque and the first component of NH sea level pressure variability (Figure 4a). In the model the mountain torque and the AO present significant coherencies at periodicities below 50 days, i.e., over a substantially larger band than in the reanalysis (Figure 4b). The fact that the mountain torque can affect the AO evolution follows that the mountain torque and the AO index are in lead-lag relationship, with the torque leading in near quadrature. It can either mean that positive (negative) values of T_M have a tendency to precede positive (negative) values of the AO or/and that negative (positive) values of the T_M have a tendency to follow positive (negative) values of the AO.

[42] To precisely determine which signal follows the other and which sign of the mountain torque is predominant, we have proceeded in section 3 with several composite analysis. As the AO is a pattern of low-frequency variability and as the cross-spectral analysis only shows significant relationships at periodicities below 50 days in the model and below 30 days in the reanalysis, we have limited the composite analysis to the conventional 10–150-day intraseasonal band [*Ghil and Mo*, 1991].

[43] The composites of SLP maps in Figures 5 and 6 reveal several important results. First, the extrema in the mountain torque T_M are associated with SLP dipoles across the Rockies and the Himalayas that are rather substantial in amplitude (around 10 hPa from minima to maxima) and significant at the 1% level (Figure 5b). These dipoles are comparable with those from the reanalysis (see Figure 5a of *Lott et al.* [2004]), witnessing that comparable mechanisms produce the mountain torque in the model and in the reanalysis. Second, the mountain torque induces circulation changes that are rather substantial and significant in the NH. In large zones, north of 30°N, the circulation is predominantly cyclonic before a negative torque (Figure 5a) and anticyclonic after (Figure 5c). Again, this is consistent with what occurs in the reanalysis data. Note, nevertheless, that in the model there is an asymmetry between negative and positive mountain torque anomalies, the former being often larger in amplitude than the later. Accordingly, the patterns in Figures 5a and 5b essentially result from flow decelerations associated with negative mountain torques.

[44] The composites of SLP maps in Figure 6 show that the negative IS AO anomalies in the model are preceded by a SLP pattern that can lead to a substantial negative mountain torque (Figure 6a), while at positive lag, the relationship with the mountain torque is less clear (Figure 6c). In the model, it is thus essentially negative phases of the AO that have a negative IS mountain torque precursor.

[45] The fact that the model AO can be moved back and forth by the mountain torque is established more quantitatively by two other pieces of evidence. First we measure the "inertia" of the AO, by calculating the mass AAM that corresponds to the EOF 1 pattern in Figure 2a. When we multiply this value by the AO index standard deviation, the value obtained is comparable in magnitude but substantially smaller than the standard deviation of M_Ω. If the variations in M_Ω are driven by the mountain torque, then the mountain torque is large enough to affect the AO substantially.

[46] The composites of the AAM budget keyed to minus the IS AAO in Figure 7a confirm this last hypothesis. They show that M_Ω decreases before a minimum in the IS AO and increases after it. These variations are near those in total AAM M, the tendencies of the wind term M_R being small (which was dynamically explained by *Lott and D'Andrea* [2005]), and almost entirely due to the mountain torque (the frictional torque being small). Note here that the positive signal in the IS mountain torque after the negative IS AO is smaller than the negative torque signal before, consistent with the results in Figure 6. Except for this last point, all these results are also consistent with those found in the reanalysis (Figure 7b).

[47] Despite some qualitative differences, the model thus confirms the results of *Lott et al.* [2004] and *Lott and D'Andrea* [2005], which link the mountain torque and the Arctic Oscillation via the mass angular momentum term.

[48] It is interesting to note that the Southern Hemisphere provides a null hypothesis for these findings. Indeed, the variability in the SH is also dominated by an annular mode, the AAO, that corresponds to a redistribution of mass from the polar regions to the midlatitudes and subtropics. Hence variations in the AAO also result in variations in mass AAM. Nevertheless, as there are many fewer mountain ranges in the SH, those variations cannot be related to the mountain torque as well as they are in the NH. This point has been extensively verified throughout the paper and in the model, as well as in the reanalysis.

[49] First, the spectral coherency between the mountain torque and the AAO are almost never significant (Figure 4), while the spectral coherency between M_Ω and the AAO is nearly always significant. Second, the mass AAM variations that occur when the IS AAO varies are in good part equilibrated by variations of opposite sign in wind AAM (for the model and the reanalysis, see Figure 8).

[50] The results presented here confirm that the mountain torque plays an active role in the NH intraseasonal vari-

ability. Since the mountain torque produces significant changes in the AO, it can have a predictive value. Nevertheless, it is important to stress the fact that the links between the mountain torque and the AO we find here are rather small; the coherency numbers in Figure 4 are in general below 0.4 and for periodicities around and below 1 month. This means that T_M can at best explain 16% of the AO variability that occurs during those periods (it is the squared coherency that matters in this respect). Furthermore, the AO is also a pattern of interannual variability, which means that a good part of its changes occur on timescales longer than a month. For these reasons and also because the mountain torque is only one among the many other dynamical processes that affect the AO, its predictive value still remains to be evaluated. The results of this paper show that general circulation models can be used for this purpose.

[51] Although we have only briefly discussed the significance of the subgrid-scale orography parameterization in the AAM budget, its small impact was rather disappointing. Indeed, the *Lott and Miller* [1997] scheme used here is rather efficient in improving the LMDz NH climatology [*Lott*, 1999], at least concerning the steady planetary waves and the zonal mean winds. It seems here that global AAM budget studies are of little help in tuning such schemes. This is rather unfortunate because there are no global data sets that document the small-scale mountain drag all around the globe: It would have been useful to find substantial relationships between the SSO torque and the AAM, because the AAM affects the length of the day that is measured routinely. Nevertheless, in this work, we did not carry out sensitivity tests of the global AAM budget to changes in the parameters of the *Lott and Miller* [1997] scheme. They may have an indirect impact on the mountain torque, for instance, that still remains to be evaluated.

[52] **Acknowledgment.** We thank Fabio D'Andrea for helpful discussions.

References

Blackmon, M. L. (1976), A climatological study of the 500 mb geopotential height of the Northern Hemisphere, *J. Atmos. Sci.*, *33*, 1607–1623.

Blackmon, M. L., and N. C. Lao (1980), Regional characteristics of the Northern Hemisphere wintertime circulation: A comparison of the simulation of the GFDL general circulation model with observations, *J. Atmos. Sci.*, *37*, 497–514.

Charney, J., and J. G. DeVore (1979), Multiple flow equilibria in the atmosphere and blocking, *J. Atmos. Sci.*, *36*, 1205–1216.

Ghil, M., and K. Mo (1991), Intraseasonal oscillations in the global atmosphere. Part I: Northern Hemisphere and tropics, *J. Atmos. Sci.*, *48*, 752–779.

Hoskins, B. J., I. N. James, and G. H. White (1983), The shape, propagation and mean-flow interaction of large-scale weather systems, *J. Atmos. Sci.*, *40*, 1595–1612.

Huang, H. P., P. D. Sardeshmuk, and K. M. Weickmann (1999), The balance of global angular momentum in a long-term atmospheric data set, *J. Geophys. Res.*, *104*(D2), 2031–2040.

Illari, L., and J. C. Marshall (1983), On the interpretation of eddy fluxes during a blocking episode, *J. Atmos. Sci.*, *40*, 2232–2242.

Kalnay, E., et al. (1996), The NCEP/NCAR 40-year reanalysis project, *Bull Am. Meteorol. Soc.*, *77*, 437–472.

Legras, B., and M. Ghil (1985), Persistent anomalies, blocking and variations in atmospheric predictability, *J. Atmos. Sci.*, *42*, 433–471.

Lejenäs, H., and R. A. Madden (2000), Mountain torques caused by normal-mode global Rossby waves, and the impact on atmospheric angular momentum, *J. Atmos. Sci.*, *57*, 1045–1051.

Lott, F. (1999), Alleviation of stationary biases in a GCM through a mountain drag parametrization scheme and a simple representation of mountain lift forces, *Mon. Weather Rev.*, *127*, 788–801.

Lott, F., and F. D'Andrea (2005), Mass and wind axial angular momentum responses to mountain torques in the 1–25 day band: Links with the Arctic Oscillation, *Q. J. R. Meteorol. Soc.*, *131*, 1483–1500.

Lott, F., and M. Miller (1997), A new subgrid scale orographic drag parameterization; its testing in the ECMWF model, *Q. J. R. Meteorol. Soc.*, *123*, 101–127.

Lott, F., A. W. Robertson, and M. Ghil (2001), Mountain torques and atmospheric oscillations, *Geophys. Res. Lett.*, *28*, 1207–1210.

Lott, F., A. W. Robertson, and M. Ghil (2004), Mountain torques and Northern-Hemisphere low-frequency variability Part I: Hemispheric aspects, *J. Atmos. Sci.*, *61*, 1259–1271.

Metz, W. (1985), Wintertime blocking and mountain forcing of the zonally averaged flow: A cross-spectral time series analysis of observed data, *J. Atmos. Sci.*, *42*, 1880–1892.

Molteni, F., S. Tibaldi, and T. Palmer (1990), Regimes in the wintertime circulation over northern extratropics. Part I: Observational evidence, *J. Atmos. Sci.*, *47*, 31–67.

Papoulis, A. (1973), Minimum bias windows for high resolution spectral estimates, *IEEE Trans. Inf. Theory*, *19*, 9–12.

Preisendorfer, R. W. (1988), *Principal Component Analysis in Meteorology and Oceanography*, 425 pp., Elsevier, New York.

Rosen, R. D. (1993), The axial momentum balance of Earth and its fluid envelope, *Surv. Geophys.*, *14*, 1–29.

Sawyer, J. S. (1976), Observational characteristics of atmospheric fluctuations with a time scale of a month, *Q. J. R. Meteorol. Soc.*, *96*, 610–625.

Vautard, R., B. Legras, and M. Déqué (1988), On the source of midlatitude low-frequency variability. Part I: A statistical approach to persistence, *J. Atmos. Sci.*, *45*, 2811–2843.

von Storch, J.-S. (1994), Interdecadal variability in a global coupled model, *Tellus, Ser. A*, *46*, 419–432.

von Storch, J.-S. (1999), The reddest atmospheric modes and the forcing of the spectra of these modes, *J. Atmos. Sci.*, *56*, 1614–1626.

Wallace, J. M. (2000), North Atlantic Oscillation/annular mode: Two paradigms–one phenomenon, *Q. J. R. Meteorol. Soc.*, *126*, 791–806.

Yoden, S. (1985), Multiple stable states of quasi-geostrophic barotropic flow over sinusoidal topography, *J. Meteorol. Soc. Jpn.*, *63*, 1031–1045.

L. Goudard, F. Lott, and A. Martin, Laboratoire de Météorologie Dynamique, Ecole Normale Supérieure, 24 rue Lhomond, F-75235 Paris Cédex 05, France. (laure.goudard@ens-lyon.fr; flott@lmd.ens.fr; martin@lmd.ens.fr)